




Molecular Stokes-Einstein and Stokes-Einstein-Debye relations for water including viscosity-dependent slip and hydrodynamic radius

Sina Zendehroud , Jan O. Daldrop, Yann von Hansen, Henrik Kiefer , and Roland R. Netz 
Freie Universität Berlin, Department of Physics, 14195 Berlin, Germany



(Received 8 July 2024; accepted 26 July 2024; published 24 December 2024)

We perform molecular dynamics simulations of liquid water at different temperatures and calculate the water viscosity, the translational and rotational water diffusivities in the laboratory frame as well as in the comoving molecular frame. Instead of interpreting the results as deviations from the Stokes-Einstein and Stokes-Einstein-Debye relations, we describe the translational and rotational diffusivities of water molecules by three models of increasing complexity that take the structural anisotropy of water into account on different levels. We first compare simulation results to analytical predictions for a no-slip sphere and a no-slip ellipsoid. We show that the no-slip sphere can approximate laboratory-frame isotropic translational and rotational diffusivities but fails to describe the anisotropic molecular-frame diffusivities. The no-slip ellipsoid can describe the translational anisotropic molecular-frame diffusivities exactly but fails to describe the translational and rotational anisotropic molecular-frame diffusivities simultaneously. Since an ellipsoidal model with slip boundary conditions is not analytically tractable, we define a heuristic spherical model with tensorial slip lengths and tensorial hydrodynamic radii. We show that this model simultaneously describes the laboratory-frame isotropic translational and rotational diffusivities, as well as, in a restricted viscosity range, the anisotropic molecular-frame diffusivities.

DOI: [10.1103/PhysRevE.110.064610](https://doi.org/10.1103/PhysRevE.110.064610)

I. INTRODUCTION

The Stokes-Einstein (SE) and the Stokes-Einstein-Debye (SED) relations predict the translational and rotational diffusivities of a sphere in a continuous viscous medium and thus describe how a macroscopic spherical body moves in fluids in the long-time limit [1–4]. According to these relations, the diffusivities are inversely linearly proportional to the solution viscosity. The putative failure of these relations to describe molecular diffusion in liquids and, in particular, deviations from the linear viscosity dependence have been intensely and controversially discussed [5–12]. It was suggested early that the SE and SED relations can be reconciled with experimental data by defining a viscosity-dependent slip length [13–15]. Likewise, it has been pointed out that the SE relation can be interpreted as a definition of the hydrodynamic radius, which thereby would acquire a dependence on temperature, particle type and solvent properties [6]. Experimentally, translational diffusivities of molecules in liquids can be accurately and consistently measured by various techniques [16]. Rotational molecular diffusivities have been derived from the fluorescence quantum yield of dyes [17], depolarized Rayleigh scattering [13], dielectric relaxation times [15], spin relaxation rates [8], and Kerr-effect spectroscopy [9]. One problem is that the rotational dynamics of molecules exhibits a slow crossover from ballistic motion at short times

to diffusive motion at long times, and that it is experimentally difficult to reach the long-time diffusive behavior where one can expect steady-state linear hydrodynamic predictions to hold (as we demonstrate later). Besides, most molecules are not spherically symmetric and therefore the translational and rotational diffusivities are anisotropic in the molecular frame. This indeed is the case for water, see Fig. 1(a), which has been at the focus of previous discussions and is the subject of the present paper. Carefully designed simulations are thus crucial, because they allow analyzing water dynamics in the molecular frame for all time scales, encompassing the crossover from ballistic to diffusive behavior.

Molecular dynamics (MD) simulation studies have reported translational and rotational diffusivities of different water models along and around the three molecular axes [18–20]. In one work the relation between the translational diffusivity and viscosity for water at varying temperature has been addressed [21]. However, a full exploration of the relation between translational and rotational diffusivities and viscosity is missing in literature.

The organization of this paper is as follows: In Sec. II, we establish the methodological framework of our study. In Sec. II A, we revisit the SE and SED relations for ellipsoidal particles with stick boundary conditions as well as spherical particles with both stick and finite slip boundary conditions. After giving details on our simulation protocol and the extraction of viscosities from our simulations in Sec. II B, we outline our method for determining molecular-frame translational and rotational diffusivities in Sec. II C. In Sec. III, we present our results and discuss the implications of our findings. We determine in Sec. III A the viscosity and the molecular-frame rotational and translational diffusivities of liquid water for a

Published by the American Physical Society under the terms of the Creative Commons Attribution 4.0 International license. Further distribution of this work must maintain attribution to the author(s) and the published article's title, journal citation, and DOI.

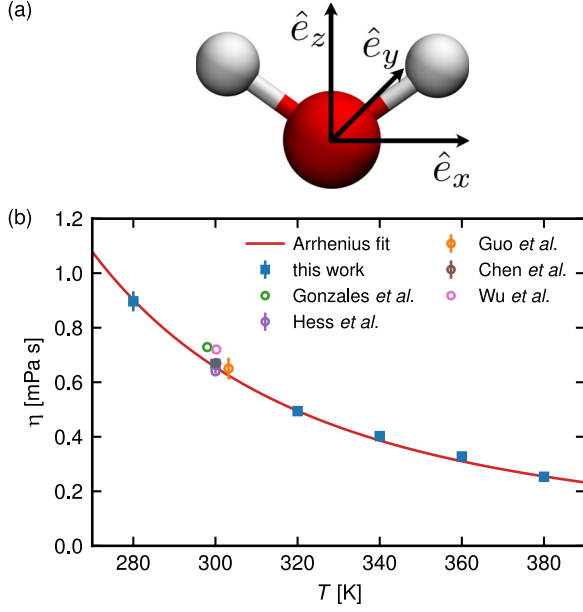


FIG. 1. (a) The molecular coordinate system (the so-called Eckart frame [45]) we use for water. (b) Our simulated water shear viscosity as a function of temperature in comparison with previous simulations around 300 K [40–44,46].

wide temperature range. Subsequently, we characterize the molecular water rotational and translational diffusivities by three models of increasing complexity that take the structural anisotropy of water into account on different levels: After a short discussion of the hydrodynamic radii following from the SE and SED relations for a spherical model with stick boundary conditions in Sec. III B 1, we show in Sec. III B 2 that the anisotropic translational diffusivity of a water molecule can be described by an ellipsoidal model with stick boundary conditions, whereas it is not possible to describe the anisotropic rotational and translational diffusivities simultaneously via this model. Finally, in Sec. III B 3, we show that the SE and SED relations can be simultaneously satisfied for low temperatures by fitting viscosity-dependent anisotropic hydrodynamic radii and slip lengths for a spherical model to the data. While this does not prove that hydrodynamics works down to molecular length scales, it shows that previous attempts to demonstrate the violation of the SE and SED relations are often unwarranted and that molecular anisotropy as well as appropriate boundary conditions are crucial for the success of future hydrodynamic models on molecular scales.

II. METHODS

A. Stokes-Einstein and Stokes-Einstein-Debye relations

1. Ellipsoid with stick boundary conditions

The diffusivity of a particle in a viscous fluid is given by the Einstein relation $D = k_B T / \zeta$ [22], where we have replaced the mobility μ by the friction coefficient $\zeta = 1/\mu$. Using the Stokes friction for the translations of a general ellipsoid with stick boundary conditions [23], the SE relations along the principal axes of the ellipsoid, denoted by superscripts x , y ,

z , read

$$\begin{aligned} D_t^x &= \frac{k_B T (\chi_0 + r_x^2 \alpha_0)}{16\pi \eta r_x r_y r_z} \\ D_t^y &= \frac{k_B T (\chi_0 + r_y^2 \beta_0)}{16\pi \eta r_x r_y r_z} \\ D_t^z &= \frac{k_B T (\chi_0 + r_z^2 \gamma_0)}{16\pi \eta r_x r_y r_z}, \end{aligned} \quad (1)$$

where r_x , r_y , r_z are the semiaxes of the ellipsoid, η is the fluid shear viscosity, and $\chi_0(r_x, r_y, r_z)$, $\alpha_0(r_x, r_y, r_z)$, $\beta_0(r_x, r_y, r_z)$, $\gamma_0(r_x, r_y, r_z)$ are elliptic integrals; see Sec. S1 in the Supplemental Material (SM) [24] for details. Analogously, the SED relations for the rotational diffusivities around the principal axes of the ellipsoid read [23]

$$\begin{aligned} D_r^x &= \frac{3k_B T (r_y^2 \beta_0 + r_z^2 \gamma_0)}{16\pi \eta r_x r_y r_z (r_y^2 + r_z^2)} \\ D_r^y &= \frac{3k_B T (r_x^2 \alpha_0 + r_z^2 \gamma_0)}{16\pi \eta r_x r_y r_z (r_x^2 + r_z^2)} \\ D_r^z &= \frac{3k_B T (r_x^2 \alpha_0 + r_y^2 \beta_0)}{16\pi \eta r_x r_y r_z (r_x^2 + r_y^2)}. \end{aligned} \quad (2)$$

Given the viscosity η as well as the diffusivities in the molecular frame (defined in Sec. II C), the effective values of the semiaxes r_x , r_y , r_z can be extracted via a least-squares fit of the data to Eqs. (1) or (2), or a combination of both. We fit the data using the Levenberg-Marquardt algorithm [25], where we choose initial values from a three-dimensional grid. The main questions are whether a unique global minimum exists and whether the obtained values for the hydrodynamic radii are reasonable and indeed solve the SE and SED relations.

Even though the SE and SED relations cannot be solved in closed form for general ellipsoids, one can gain some intuition by considering the case of a slightly deformed sphere. In this case, we let $r_0 := r_x = r_y$ and $r_z = r_0(1 + \epsilon)$ with $|\epsilon| \ll 1$. The SE and SED relations Eq. (1) and Eq. (2), respectively, are expanded in terms of ϵ up to first order. The SE relation for the translational diffusivity then reads

$$\begin{aligned} D_t^{x,y} &\simeq \frac{k_B T}{6\pi \eta r_0} \left(1 + \frac{2}{5}\epsilon\right) \\ D_t^z &\simeq \frac{k_B T}{6\pi \eta r_0} \left(1 + \frac{1}{5}\epsilon\right), \end{aligned} \quad (3)$$

whereas the SED relation for the rotational diffusivity reads

$$\begin{aligned} D_r^{x,y} &\simeq \frac{k_B T}{8\pi \eta r_0^3} \left(1 + \frac{6}{5}\epsilon\right) \\ D_r^z &\simeq \frac{k_B T}{8\pi \eta r_0^3} \left(1 + \frac{1}{5}\epsilon\right). \end{aligned} \quad (4)$$

From Eqs. (3) and (4), one can see that the deformation of a sphere along a single axis impacts both the translational and rotational diffusivities along (around) the perpendicular axes more strongly than along (around) the same axis. This effect is more pronounced for the rotational diffusivities and will be relevant for our modeling later on.

2. Sphere with finite slip

The SE expression for the translational diffusivity of a spherical particle with a general slip boundary condition is given by [22,26]

$$D_t = \frac{k_B T}{6\pi\eta r f_t}, \quad (5)$$

where r is the hydrodynamic sphere radius and η the fluid shear viscosity. The slip correction factor is $f_t = \frac{1+2b/r}{1+3b/r}$ [27] and depends on the slip length b , which is related to the surface friction coefficient λ via $b = \eta/\lambda$ [28]. In the stick limit ($b/r = 0$) one has $f_t = 1$ and in the slip limit ($b/r \rightarrow \infty$ as realized for bubbles) one has $f_t \rightarrow 2/3$. Analogously, the SED expression for the rotational sphere diffusivity reads [22,26,29]

$$D_r = \frac{k_B T}{8\pi\eta r^3 f_r} \quad (6)$$

with the correction factor given by $f_r = \frac{1}{1+3b/r}$ [27] with the limits $f_r = 1$ for $b/r = 0$ and $f_r \rightarrow 0$ for $b/r \rightarrow \infty$. For molecules one expects finite correction factors f_t and f_r with values between the asymptotic limits [13,14].

Based on translational and rotational diffusivity data the hydrodynamic radius and slip length can be extracted as follows: Combining Eqs. (5) and (6) leads to

$$\frac{D_r}{D_t^3} = 27\pi^2 (k_B T)^{-2} \eta^2 \frac{f_t^3}{f_r}, \quad (7)$$

which only depends on the ratio r/b . Knowing the viscosity, r/b can thus be obtained from the ratio D_r/D_t^3 by numerical inversion, though it is not *a priori* clear whether a solution exists. Having determined r/b the hydrodynamic radius r then follows from Eqs. (5) or (6). Again, the main questions are whether the inversion is possible and whether the obtained values for r and b are reasonable. Note that since Eq. (7) is a third-order equation in b/r , inversion is possible analytically. As a check, we numerically evaluate Cardano's formula for Eq. (7) and find identical solutions. Note furthermore that third-order equations can have up to three solutions. In our case, if inversion with positive hydrodynamic radius r is possible, then there are two solutions, one with positive and one with negative slip length. In the following, always the solution with positive slip length b is considered. The solutions involving negative slip lengths are shown in Sec. S10 in the SM [24].

B. Molecular dynamics simulations

We here calculate translational and rotational diffusivities from 10 ns long MD simulation trajectories of $N = 1410$ SPC/E water molecules [30] in a mean volume of roughly $V = (3.5 \text{ nm})^3$ using the GROMACS 4.6 simulation package [31–35] with a time step of $\Delta t = 2 \text{ fs}$. We use a Parrinello-Rahman barostat [36,37] at 1 bar and a velocity-rescaling thermostat [38]. We vary the water shear viscosity by changing the temperature T from 280 K to 380 K in steps of 20 K.

The water viscosity η is determined from momentum fluctuations [39,40] using extended trajectories of 300 ns (see Sec. S2 and S3 in the SM for details [24]) and is shown as a

function of temperature in Fig. 1(b). In agreement with experiments, η decreases drastically with increasing temperature, which demonstrates that the SE and SED relations can be sensitively probed in pure water by changing temperature. We favorably compare our results for η in Fig. 1(b) to previous simulation results around 300 K [40–44]. An Arrhenius fit of η according to $\eta(T) = \eta_0 \exp(E_\eta/k_B T)$ with $\eta_0 = (7.4 \pm 0.6) \times 10^{-3} \text{ mPa s}$ and $E_\eta = (11.2 \pm 0.2) \text{ kJ/mol}$ [red line in Fig. 1(b)] describes the data rather well, which suggests that the viscosity involves a thermally assisted barrier crossing process.

C. Molecular-frame translational and rotational diffusivities

To obtain molecular-frame translational diffusivities, we first project the laboratory-frame water displacement $\Delta \mathbf{r}(t) = \mathbf{r}(t) - \mathbf{r}(0)$, where $\mathbf{r}(t)$ is the oxygen position of a given water molecule at time t , onto the comoving molecular coordinate frame according to [18,19]

$$\Delta \boldsymbol{\alpha}(t) = \sum_{i=1}^{t/\Delta t} [(\mathbf{r}(i\Delta t) - \mathbf{r}((i-1)\Delta t)) \cdot \hat{\boldsymbol{\epsilon}}_\alpha^{(i-1/2)}] \hat{\boldsymbol{\epsilon}}_\alpha^{(i-1/2)}, \quad (8)$$

where $\alpha \in \{x, y, z\}$. The unit vectors $\hat{\boldsymbol{\epsilon}}_\alpha$ in the molecular frame are shown in Fig. 1(a), and we define half-step unit vectors as $\hat{\boldsymbol{\epsilon}}_\alpha^{(i-1/2)} = (\hat{\boldsymbol{\epsilon}}_\alpha(i\Delta t) + \hat{\boldsymbol{\epsilon}}_\alpha((i-1)\Delta t))/2$. Obviously, $\Delta \mathbf{r}(t) = \sum_\alpha \Delta \boldsymbol{\alpha}(t)$. Using Eq. (8), we define the translational mean-squared displacement (MSD) matrix as

$$\mathcal{M}_{\alpha\beta}(t) = \langle (\Delta \boldsymbol{\alpha}(t + \tau) - \Delta \boldsymbol{\alpha}(\tau)) \cdot (\Delta \boldsymbol{\beta}(t + \tau) - \Delta \boldsymbol{\beta}(\tau)) \rangle, \quad (9)$$

where $\alpha, \beta \in \{x, y, z\}$ and the average is calculated over all water molecules and reference times τ . We next define the translational MSDs in the molecular frame by partial summation as

$$\langle \Delta r_\alpha^2(t) \rangle = \sum_\beta \mathcal{M}_{\alpha\beta}(t), \quad (10)$$

so that the laboratory-frame MSD is recovered by $\langle \Delta r^2(t) \rangle = \sum_\alpha \langle \Delta r_\alpha^2(t) \rangle$. Note that translational molecular-frame MSDs were previously defined as the diagonal components $\mathcal{M}_{\alpha\alpha}$ [18–20], which show distinct scaling behavior compared to the laboratory-frame MSD. This demonstrates the relevance of the off-diagonal components of \mathcal{M} , in particular when the validity of the SE relation is concerned; see Sec. S4 in the SM [24].

The rotational MSDs around the molecular axes are calculated according to [18,19]

$$\langle \Delta \varphi_\alpha^2(t) \rangle = \langle (\Delta \varphi_\alpha(t + \tau) - \Delta \varphi_\alpha(\tau))^2 \rangle \quad (11)$$

with the angular displacements defined as

$$\Delta \varphi_\alpha(t) = \sum_{i=1}^{t/\Delta t} \frac{1}{2} \sum_{\beta, \gamma} \varepsilon_{\alpha\beta\gamma} \hat{\boldsymbol{\epsilon}}_\beta(i\Delta t) \cdot \hat{\boldsymbol{\epsilon}}_\gamma((i-1)\Delta t) \quad (12)$$

for $\alpha, \beta, \gamma \in \{x, y, z\}$ and where $\varepsilon_{\alpha\beta\gamma}$ denotes the three-dimensional Levi-Civita symbol [47]. The translational diffusivities in the laboratory and molecular frame follow from the MSDs as $D_t^{\text{lab}} = \lim_{t \rightarrow \infty} \langle \Delta r^2 \rangle / 6t$ and

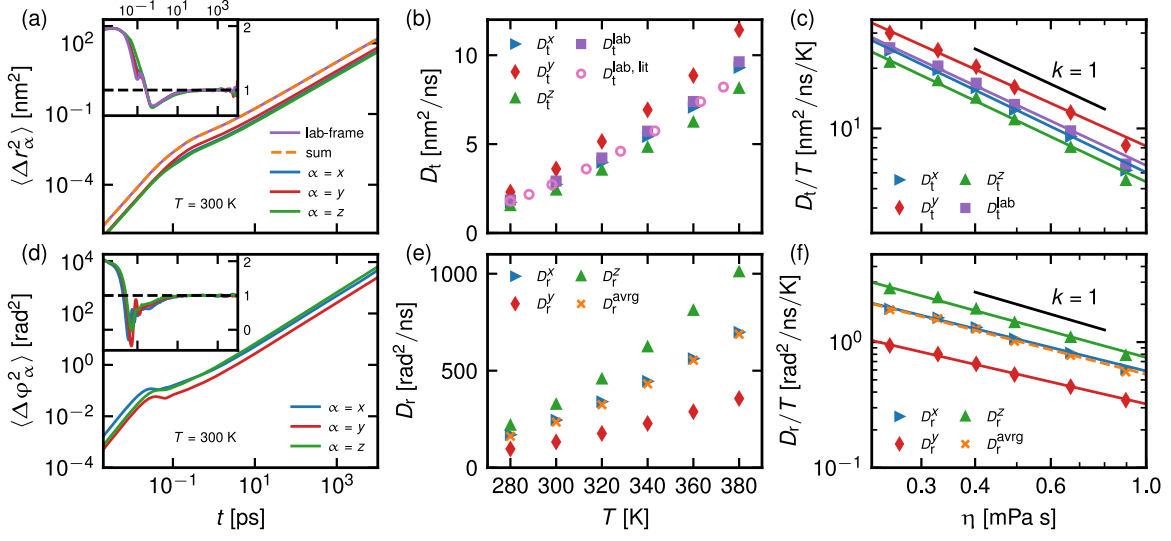


FIG. 2. (a) Translational and (d) rotational MSDs for SPC/E water at $T = 300$ K. The insets show the time-dependent MSD power-law exponent, which is 2 for ballistic and 1 for diffusive motion. (b) Translational diffusivities as a function of temperature in the laboratory frame, D_t^{lab} , and along the molecular axes, $D_t^{x,y,z}$. For reference, the laboratory-frame translational diffusivity of SPC/E water from Ref. [44] is included. (e) Rotational diffusivities around the molecular axes, $D_r^{x,y,z}$, and its average D_r^{avg} . (c) Corresponding translational and (f) rotational rescaled diffusivities as a function of the viscosity η . Fits according to $D_{r,t}/T \sim \eta^{-k}$ are shown as solid lines. The power-laws $k = 1$ are indicated by black straight lines.

$D_t^\alpha = \lim_{t \rightarrow \infty} \langle \Delta r_\alpha^2 \rangle / 2t$, the rotational diffusivities are given by $D_r^\alpha = \lim_{t \rightarrow \infty} \langle \Delta \varphi_\alpha^2 \rangle / 2t$ for $\alpha \in \{x, y, z\}$.

Note that, since the SPC/E water model is nonorthotropic, couplings between the translational and rotational diffusivities described by the coupling coefficients $D_{t,r}^{\alpha\beta} = D_{r,t}^{\beta\alpha} = \lim_{t \rightarrow \infty} \langle \Delta r_\alpha(t) \Delta \varphi_\beta(t) \rangle / 2t$ are expected and enter the description as nondiagonal elements in the grand-diffusivity matrix [48,49]. As we aim to describe water diffusivities by analytically tractable orthotropic models, these couplings are not considered in the present work, but can be included in future studies.

III. RESULTS

A. Translational and rotational diffusivities

The simulated laboratory and molecular translational MSDs as well as the rotational MSDs according to Eqs. (10) and (11) are shown in Figs. 2(a) and 2(d) for an exemplary temperature of $T = 300$ K, results for different temperatures are given in Sec. S5 in the SM [24]. One observes a slow crossover from ballistic to diffusive behavior, which is illustrated by the time-dependent MSD power-law exponent in the insets, which changes from 2 for short times to 1 for long times. The sum of all molecular translational MSDs (orange broken line) perfectly overlaps with the laboratory-frame MSD (purple line) in Fig. 2(a), as expected.

The diffusivities are calculated from the MSDs by linear fits in the time interval from 100 ps to 1000 ps, where the data exhibit diffusive behavior, and are corrected for hydrodynamic finite-size effects [50,51] (see Sec. S6 in the SM [24] for details). Recently, a frequency-dependent finite-size correction to the diffusivity has been proposed in Ref. [52]. The results following from uncorrected data are shown in Sec. S11 in the SM [24]. In the time range we use for the fits, SPC/E

water behaves as a Newtonian Markovian fluid and a possible frequency dependence of the viscosity in Eqs. (5) and (6) can be neglected [53]. The results in Figs. 2(b) and 2(e) show that all diffusivities increase with temperature, as expected based on the viscosity scaling in Fig. 1(b). The translational as well as the rotational diffusivities are anisotropic: For example, the translational diffusivity along the y axis D_t^y is about 1.5 times higher than D_t^z , in agreement with previous findings [18,19], the rotational diffusivity around the y axis D_r^y is reduced by roughly a factor of two compared to D_r^z , in qualitative agreement with experiments [54] and simulations [20].

In Figs. 2(c) and 2(f), the rescaled diffusivities D/T are plotted against the viscosity η together with power-law fits according to $D/T \sim \eta^{-k}$, the fitted exponents k are listed in Table I. According to Eqs. (5) and (6) one would expect $k = 1$ for viscosity-independent radius r and slip length b . In fact, the laboratory-frame translational diffusivity data in Fig. 2(c) are in perfect agreement with $k = 1$. The molecular anisotropic translational diffusivities are within their errors consistent with $k = 1$ as well. This is in agreement with

TABLE I. The exponents k from the fits of the translational and rotational diffusivities to the viscosity according to $D/T \sim \eta^{-k}$.

		k
Lab frame translation	D_t^{lab}	1.00 ± 0.06
Molecular translations	D_t^x	1.04 ± 0.06
	D_t^y	0.96 ± 0.06
	D_t^z	1.02 ± 0.07
	D_r^{avg}	0.88 ± 0.04
Molecular rotations	D_r^x	0.85 ± 0.04
	D_r^y	0.79 ± 0.03
	D_r^z	0.94 ± 0.05
	D_r^{avg}	0.88 ± 0.04

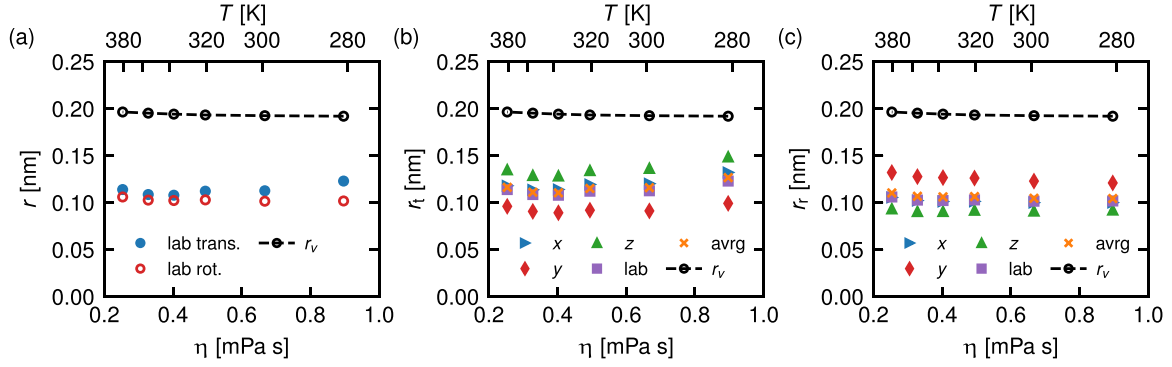


FIG. 3. (a) Hydrodynamic laboratory-frame radii r_t^{lab} (filled blue circles) and r_r^{lab} (open red circles) for the translational and rotational diffusion of a water molecule as a function of the viscosity η . The radii are calculated via Eq. (13) using D_t^{lab} and D_r^{avg} , respectively. (b), (c) Axis-specific hydrodynamic radii r_t^α (b) and r_r^α (c) from the anisotropic translational and rotational diffusion of a water molecule as a function of the viscosity η , calculated via Eq. (13). $r_{t,r}^\alpha$ is calculated from $D_{t,r}^\alpha$ for $\alpha \in \{x, y, z\}$. r_{avg} denotes the average of the results for r over all axes. The laboratory-frame results from subfigure (a) are included as purple squares. For comparison, in (a)–(c), the geometric water radius r_v is included as black circles linearly interpolated by a dashed line.

previous simulation studies [7,10,11] and experiments [55]. In contrast, some simulations reported smaller exponents, as reviewed recently [56], which has been argued to be due to the different simulation methods used to estimate the shear viscosity [11].

The molecular rotational diffusivities in Fig. 2(f) exhibit significantly lower exponents, the diffusivity D_r^{avg} averaged over all three directions is characterized by $k \approx 0.88$ (see Table I), which indicates significant deviations from the SED relation. In related MD simulations, the rotational diffusivity of the water dipole vector in the laboratory frame was found to be characterized by an exponent $k = 0.75$, not so far from our result [57]. Note, however, that in these simulations a different definition of the angular displacement was used and the viscosity was estimated from the relaxation time of the coherent intermediate scattering function [57]. Also, in that work, the exponent k was estimated from a fit according to $D \sim (T/\eta)^k$ in contrast to our definition $D/T \sim \eta^{-k}$, which follows from the definition of the SE and SED relations in Eqs. (5) and (6). In Sec. S7 in the SM [24] we show that the deviation in k between these two different fit expressions is however rather small.

B. Hydrodynamic radii and slip lengths

In the following we will describe the molecular water rotational and translational diffusivities by three models of increasing complexity that take the structural and slip anisotropy of water into account on different levels. Analytical results are only available for orthotropic models, we therefore cannot regard translational-rotational couplings in the diffusivities, as briefly mentioned in Sec. II C.

1. Sphere with stick boundary conditions

The SE and SED relations for a spherical particle with stick boundary conditions in a viscous fluid are given by Eqs. (5) and (6), where the corresponding slip correction factors are set to one, i.e., $f_t = f_r = 1$. Rearranging these equations for

r , it is easy to define hydrodynamic radii

$$r_t = \frac{k_B T}{6\pi\eta D_t}, \quad r_r = \left(\frac{k_B T}{8\pi\eta D_r} \right)^{1/3}, \quad (13)$$

for the translational and rotational diffusion along the molecular frame axes, respectively. Although Eq. (13) is derived for an isotropic sphere, we heuristically use the expression to define different radii in the different directions of the molecular frame.

In Fig. 3(a), we show the hydrodynamic radii r_t^{lab} and r_r^{lab} for the translational and rotational diffusion of SPC/E water in the laboratory frame following from the diffusivities D_t^{lab} and D_r^{avg} obtained in Sec. III A, respectively. We include for comparison the slightly temperature-dependent geometric radius r_v , which is the radius of a sphere with the molecular volume $v = V/N$ of a water molecule, where V is the mean volume of the simulation box and N is the number of water molecules. We find that r_t^{lab} and r_r^{lab} remain fairly constant over the whole range of viscosities and stay well below the geometric radius r_v . Furthermore, the radii for translational and rotational motion in the laboratory frame are in good agreement, with noticeable differences only arising at the highest viscosity. This suggests that the laboratory-frame diffusion of a water molecule can be well approximated by a spherical model with stick boundary conditions.

We now turn to the anisotropic molecular frame results. In Figs. 3(b) and 3(c), we show the hydrodynamic radii r_t^α and r_r^α for the translational and rotational diffusion, respectively, of a water molecule along the three molecular axes $\alpha \in \{x, y, z\}$ following from the diffusivities $D_{t,r}^\alpha$ obtained in Sec. III A. For the translational motion, see Fig. 3(b), we find that the hydrodynamic radii r_t remain fairly constant over the whole range of viscosities, and stay below the geometric radius r_v . The radii for the diffusion along the three distinct molecular axes are clearly different, where the hydrodynamic radius for translations along the z axis is largest and the radius for translations along the y axis is smallest, reflecting the anisotropy in diffusion discussed in Sec. III A.

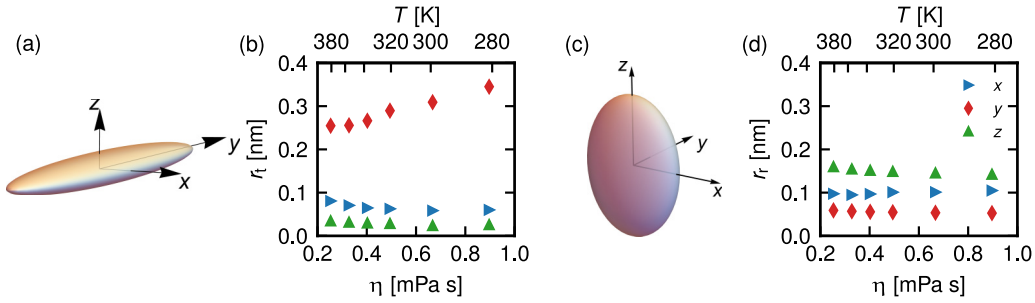


FIG. 4. (a) Sketch of ellipsoid with semiaxes corresponding to the hydrodynamic radii for the translation of a water molecule at $T = 280$ K obtained from Eq. (1). (b) Hydrodynamic radii r_t^x , r_t^y , r_t^z for the translating ellipsoid as a function of viscosity η for each axis. (c) Sketch of ellipsoid with semiaxes corresponding to best fit of the hydrodynamic radii with $r_r^\alpha > 0$, $\alpha \in \{x, y, z\}$, to the rotations of a water molecule at $T = 280$ K obtained from Eq. (2). (d) Hydrodynamic radii r_r^x , r_r^y , r_r^z for the best fitting rotating ellipsoid with $r_r^\alpha > 0$, $\alpha \in \{x, y, z\}$, as a function of viscosity η for each axis.

Regarding the rotational motion, in Fig. 3(c), we again find that the hydrodynamic radii are fairly constant over the whole range of viscosities, stay below the geometric radius r_v , and, as for the translational case, display a clear anisotropy. However, for the rotational motion, the hydrodynamic radii for rotations around the y axis are largest and the radii for rotations around the z axis are smallest. None of the radii r_t and r_r coincide for a given axis, as would be suggested by the first-order expansion in Eqs. (3) and (4). On the contrary, we note that the rotational radius along one axis corresponds approximately to the average taken over the translational radii along the two perpendicular axes, e.g., $r_r^z \approx (r_t^x + r_t^y)/2$, and vice versa (see Sec. S8 in the SM [24] for details). Nevertheless, one needs six different radii to describe the translational and rotational diffusivities in the molecular frame. This is in contrast to the results in the laboratory frame, which are both well described by a single radius. This suggests that the spherical model with stick boundary conditions is not suitable to simultaneously describe the anisotropic translational *and* rotational diffusivities of an SPC/E water molecule in the molecular frame, and generalizations are needed.

2. Ellipsoid with stick boundary conditions

Because of the shortcoming of the spherical model with stick boundary conditions, we now generalize the sphere to an ellipsoid with arbitrary semiaxes r_x , r_y , and r_z and stick boundary conditions.

We first consider the translational diffusivity of the ellipsoid. In Fig. 4(b), we show the semiaxes r_t^x , r_t^y , and r_t^z of the ellipsoid obtained from the translational diffusivities of a water molecule as a function of the solution viscosity, obtained using the method described in Sec. II A 1 via Eq. (1). The radii are unique and exactly reproduce the diffusivities extracted from our MD data, i.e., the error of the fit is zero. We find that the hydrodynamic radii r_t^x , r_t^y , and r_t^z are quite different for all viscosities. The lowest radii are found for the z axis, i.e., along the dipole axis of the water molecule, whereas the radii for the x axis are almost twice as large as r_t^z . The hydrodynamic radius in the y direction, i.e., orthogonal to the HOH-plane, is by far the largest, approximately four times as large as r_t^x and ten times with respect to r_t^z . While the radii r_t^x , and r_t^z stay fairly constant with viscosity, r_t^y steadily

increases with increasing viscosity. A sketch of the ellipsoid with semiaxes corresponding to the hydrodynamic radii for the translation of a water molecule at $T = 280$ K is shown in Fig. 4(a).

We next consider the rotational diffusivity of the ellipsoid. In contrast to the translational case, the rotating ellipsoid model Eq. (2) cannot be fit to the MD data perfectly, i.e., the error of the fit is finite. In Fig. 4(d), we show the semiaxes r_r^x , r_r^y , and r_r^z of the best fitting ellipsoid, i.e., the global minimum of the least-squares loss function with the condition that $r_r^\alpha > 0$ for $\alpha \in \{x, y, z\}$. The error of the rotational diffusivities predicted by the ellipsoidal model with respect to the MD data is shown in Sec. S9 in the SM [24]. We find that, in contrast to the translational case, the hydrodynamic radii remain fairly constant with viscosity. The hydrodynamic radii in the y direction are smallest, whereas the radii for the z axis are largest.

This is in contrast to the results in the translational case, where the semiaxis r_t^y is largest. Due to this inconsistency of shapes, cf. the sketches in Figs. 4(a) and 4(c), we conclude that also the ellipsoidal model with stick boundary conditions is not suitable to simultaneously describe the anisotropic translational *and* rotational diffusivities of an SPC/E water molecule in the molecular frame, whereas the translational motion alone is well described by the ellipsoidal model. As a consequence, we will generalize the boundary conditions in the next section.

3. Sphere with finite slip

We now depart from the assumption of stick boundary conditions and allow for finite slip. In order to increase the complexity of our model as little as possible, and since no analytical solution for the diffusivities of an ellipsoid with finite slip is available, we use a spherical model with finite slip, as is described in Sec. II A 2.

We solve Eq. (7) for the ratio r/b and obtain the hydrodynamic radius r from Eq. (5). Once the hydrodynamic radius is known, the slip length b follows from the ratio b/r . In order to check for possible anisotropies in the extracted values of the radius and the slip length, we extract hydrodynamic radii r_x , r_y , r_z and slip lengths b_x , b_y , b_z using the molecular-frame diffusivities obtained in Sec. III A. Since deformation of a sphere along one axis impacts both translational and rotational

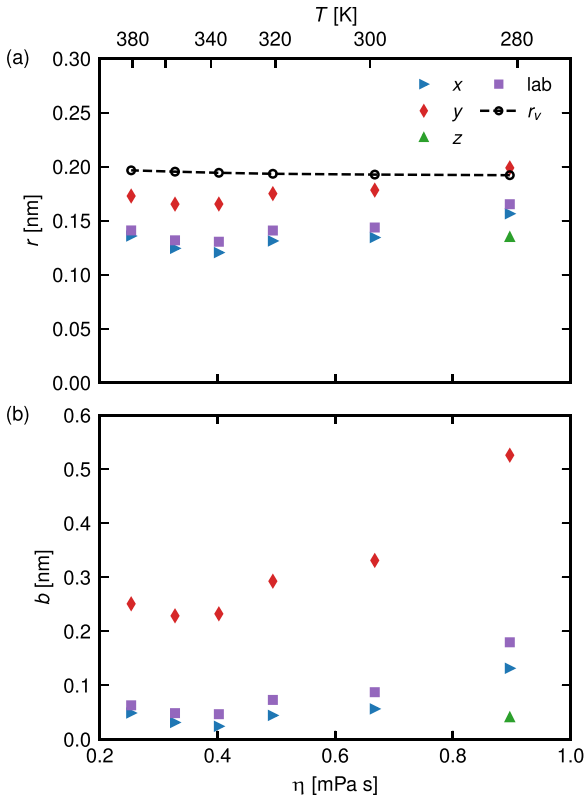


FIG. 5. (a) Hydrodynamic radii r_x , r_y , r_z and (b) slip lengths b_x , b_y , b_z obtained from Eq. (7) as a function of viscosity η for each axis. r_{lab} and b_{lab} are calculated from the translational laboratory-frame diffusivity D_t^{lab} and the average rotational diffusivity D_r^{avrg} . For comparison, the geometric water radius r_v is included in (a) as black circles linearly interpolated by a dashed line.

diffusivities along the two perpendicular axes more strongly, as follows from Eqs. (3) and (4), we extract the hydrodynamic radius and slip length for one axis by using the average diffusivities along the two perpendicular axes in Eq. (7). For example, to extract r_z and b_z , we use $D_t := (D_t^x + D_t^y)/2$ and $D_r := (D_r^x + D_r^y)/2$ in Eq. (7). The results for the hydrodynamic radii and slip lengths when using alternative combinations of diffusivities are shown in Sec. S10 in the SM [24].

In Figs. 5(a) and 5(b) the effective radii r_α and the slip lengths b_α for each axis are shown as a function of the solution viscosity. For now, we concentrate on r_{lab} and b_{lab} (purple squares). In Figs. 5(a) we include for comparison the geometric radius r_v , as introduced in Sec. III B 1. We see that the hydrodynamic radii do not change much with viscosity, except at the highest viscosities, and are slightly smaller than r_v , which is a physically intuitive result. The effective radius is more or less constant with the average $\langle r_{\text{lab}} \rangle_\eta = 0.14$ nm. For high viscosities (low temperatures) the radius increases, which one could interpret as a consequence of enhanced water binding, as one would intuitively expect. In contrast, the slip length b_{lab} varies, but stays around $b_{\text{lab}} \approx 0.1$ nm. This suggests that the translational and rotational diffusion of water in the laboratory frame can indeed be explained by a spherical model with finite slip, whereas the characterization as a sphere with stick boundary conditions holds only approximately; see Fig. 3(a).

Regarding the anisotropic molecular-frame diffusion, we find that inversion of Eq. (7) is for all axes possible only for the highest viscosity (lowest temperature), whereas for the other viscosities, inversion for r_z and b_z fails. We therefore concentrate on the results for r_x and r_y , for which inversion of Eq. (7) is possible over the whole range of viscosities. We see that the hydrodynamic radii r_x and r_y exhibit moderate anisotropy, where r_y is always larger than r_x , and, in the case where a solution for r_z is found, r_z is lowest. Interestingly, the very same hierarchy is reflected in the translating ellipsoid model with stick boundary conditions; see Fig. 4(b). Similarly to the laboratory-frame results, the radii r_x and r_y increase with higher viscosities. In comparison with the geometric radius r_v , the hydrodynamic radii r_x are smaller, whereas r_y is similar to r_v and approaches r_v with increasing viscosity. For the highest viscosity, r_y even slightly surpasses r_v . In contrast, the different slip lengths, and especially b_y , vary significantly with viscosity and exhibit a minimum at intermediate viscosity. Interestingly, the slip lengths b_x are rather similar to the hydrodynamic radius, whereas b_y is always higher than r_y , and for the highest viscosity b_y is more than twice as large as r_y . Our anisotropic results reflect that water dynamics is rather anisotropic over the whole range of viscosities η and the isotropic model described by Eqs. (5) and (6) is not suitable to describe the molecular-frame diffusion of water.

IV. CONCLUSION

In the present work, we perform molecular dynamics simulations of SPC/E water at different temperatures and calculate the viscosities as well as the rotational and translational self-diffusion constants of water molecules in the laboratory frame as well as in the anisotropic molecular frame. In the latter case, we introduce the MSD matrix and show that a complete decomposition of the translational laboratory-frame MSD into the molecular-frame MSDs is possible only if the off-diagonal components of the MSD matrix are taken into account.

We demonstrate that the translational diffusivities of SPC/E water obey the SE relation for a general ellipsoidal model with stick boundary conditions and viscosity-dependent radii. We show that neither a spherical model with stick boundary conditions nor an ellipsoidal model with stick boundary conditions can simultaneously describe the anisotropic translational and rotational diffusivities of SPC/E water. We also show that the (isotropic) translational and rotational diffusion in the laboratory frame can be only approximately described by a spherical model with stick boundary conditions.

We demonstrate that the (isotropic) translational and rotational diffusivities of SPC/E water in the laboratory frame obey the SE and SED relations if slip is taken into account for a spherical model and if both hydrodynamic radius and slip length are allowed to change with viscosity. The slip length and the hydrodynamic radius of a single water molecule have recently been determined by comparison of the frequency-dependent friction response from the transient Stokes equation and from simulations to $r = 0.14$ nm and $b = 0.10$ nm for a system at $T = 300$ K, showing good agreement with our results [58]; this lends support to our approach, which is applicable to general molecules in different solvents. Regarding the

anisotropic molecular-frame diffusion, a satisfactory description of the anisotropic diffusion in the molecular frame via a spherical model with finite slip is only possible for the highest viscosity (lowest temperature). For the other viscosities, only two of the three axes can be described by the spherical model with finite slip.

Our results suggest that continuum hydrodynamic equations remain useful down to molecular length scales, provided the appropriate boundary conditions are used, which is relevant for the growing field of nanofluidics [59]. However, our results show that the anisotropy of the molecule proves to be a crucial factor in the description of its diffusive behavior. Our findings support the idea that an ellipsoidal model with

anisotropic radii and slip lengths, i.e., six model parameters for six molecular-frame diffusivities, presumably can explain the anisotropic diffusion of water molecules in the molecular frame. We are not aware of an analytical solution for the diffusion of an ellipsoid with arbitrary slip boundary conditions, which is a topic for future research.

ACKNOWLEDGMENTS

This research has been funded by Deutsche Forschungsgemeinschaft (DFG) through Grant No. CRC 1114-235221301, Project No. C02 and Grant No. CRC 1449-431232613, Project No. A03.

-
- [1] L. D. Landau, E. M. Lifshitz, J. B. Sykes, and W. H. Reid, *Fluid Mechanics*, A-W Series in Advanced Physics (Pergamon and Addison-Wesley, Oxford and Reading, MA, 1984).
- [2] J. K. G. Dhont, *An Introduction to Dynamics of Colloids*, 2nd ed., edited by D. Möbius and R. Miller (Elsevier, Amsterdam, 2003).
- [3] T. M. Squires and T. G. Mason, Fluid mechanics of microrheology, *Annu. Rev. Fluid Mech.* **42**, 413 (2010).
- [4] A. M. Puertas and T. Voigtmann, Microrheology of colloidal systems, *J. Phys.: Condens. Matter* **26**, 243101 (2014).
- [5] G. L. Pollack and J. J. Enyeart, Atomic test of the Stokes-Einstein law. II. Diffusion of Xe through liquid hydrocarbons, *Phys. Rev. A* **31**, 980 (1985).
- [6] R. Zwanzig and A. K. Harrison, Modifications of the Stokes-Einstein formula, *J. Chem. Phys.* **83**, 5861 (1985).
- [7] L. Xu, F. Mallamace, Z. Yan, F. W. Starr, S. V. Buldyrev, and H. Eugene Stanley, Appearance of a fractional Stokes-Einstein relation in water and a structural interpretation of its onset, *Nat. Phys.* **5**, 565 (2009).
- [8] L. R. Winther, J. Qvist, and B. Halle, Hydration and mobility of Trehalose in aqueous solution, *J. Phys. Chem. B* **116**, 9196 (2012).
- [9] D. A. Turton and K. Wynne, Stokes-Einstein-Debye failure in molecular orientational diffusion: Exception or rule? *J. Phys. Chem. B* **118**, 4600 (2014).
- [10] T. Kawasaki and K. Kim, Identifying time scales for violation/preservation of Stokes-Einstein relation in supercooled water, *Sci. Adv.* **3**, e1700399 (2017).
- [11] G. Ren and Y. Wang, Conservation of the Stokes-Einstein relation in supercooled water, *Phys. Chem. Chem. Phys.* **23**, 24541 (2021).
- [12] T. Samanta and D. V. Matyushov, Dielectric friction, violation of the Stokes-Einstein-Debye relation, and non-Gaussian transport dynamics of dipolar solutes in water, *Phys. Rev. Res.* **3**, 023025 (2021).
- [13] D. R. Bauer, J. I. Brauman, and R. Pecora, Molecular reorientation in liquids: Experimental test of hydrodynamic models, *J. Am. Chem. Soc.* **96**, 6840 (1974).
- [14] K. Krynicki, C. D. Green, and D. W. Sawyer, Pressure and temperature dependence of self-diffusion in water, *Farad. Discuss. Chem. Soc.* **66**, 199 (1978).
- [15] G. Sposito, Single-particle motions in liquid water. II. The hydrodynamic model, *J. Chem. Phys.* **74**, 6943 (1981).
- [16] H. J. V. Tyrrell and K. R. Harris, *Diffusion in Liquids* (Butterworth-Heinemann, Oxford, 1984).
- [17] T. Förster and G. Hoffmann, Die Viskositätsabhängigkeit der Fluoreszenzquantenausbeuten einiger Farbstoffsysteme, *Z. Phys. Chem.* **75**, 63 (1971).
- [18] D. Rozmanov and P. G. Kusalik, Transport coefficients of the TIP4P-2005 water model, *J. Chem. Phys.* **136**, 044507 (2012).
- [19] G. Chevrot, K. Hinsén, and G. R. Kneller, Model-free simulation approach to molecular diffusion tensors, *J. Chem. Phys.* **139**, 154110 (2013).
- [20] N. Meyer, V. Piquet, J.-F. Wax, H. Xu, and C. Millot, Rotational and translational dynamics of the SPC/E water model, *J. Mol. Liq.* **275**, 895 (2019).
- [21] P. Montero de Hijes, E. Sanz, L. Joly, C. Valeriani, and F. Caupin, Viscosity and self-diffusion of supercooled and stretched water from molecular dynamics simulations, *J. Chem. Phys.* **149**, 094503 (2018).
- [22] A. Einstein, Zur Theorie der Brownschen Bewegung [AdP 19, 371 (1906)], *Ann. Phys.* **517**, 194 (2005).
- [23] S. Kim and S. J. Karrila, *Microhydrodynamics: Principles and Selected Applications* (Butterworth-Heinemann, Oxford, 1991).
- [24] See Supplemental Material at <http://link.aps.org/supplemental/10.1103/PhysRevE.110.064610> for details regarding elliptic integrals, viscosity calculations, mean-squared displacement calculations and fits, finite-size corrections, stick sphere and ellipsoid results, and slip sphere results following from alternative combinations of diffusivities, which includes Refs. [60–63].
- [25] J. J. Moré, The Levenberg-Marquardt algorithm: Implementation and theory, in *Numerical Analysis*, Lecture Notes in Mathematics No. 630, edited by G. A. Watson (Springer Verlag, Berlin, 1977), pp. 105–116.
- [26] G. G. Stokes, On the effect of internal friction of fluids on the motion of pendulums, *Mathematical and Physical Papers* (Cambridge University Press, Cambridge, 2009), pp. 1–10.
- [27] A. B. Basset, *A Treatise on Hydrodynamics: With Numerous Examples* (Dover, Mineola, NY, 1961).
- [28] L. Bocquet and E. Charlaix, Nanofluidics, from bulk to interfaces, *Chem. Soc. Rev.* **39**, 1073 (2010).
- [29] P. Debye, *Polar Molecules* (The Chemical Catalogue Company, New York, 1929).
- [30] H. J. C. Berendsen, J. R. Grigera, and T. P. Straatsma, The missing term in effective pair potentials, *J. Phys. Chem.* **91**, 6269 (1987).

- [31] H. Bekker, H. J. C. Berendsen, E. J. Dijkstra, S. Achterop, R. van Drunen, D. van der Spoel, A. Sijbers, H. Keegstra, B. Reitsma, and M. K. R. Renardus, Gromacs: A parallel computer for molecular dynamics simulations, in *Physics Computing 92*, edited by R. A. de Groot and J. Nadrchal (World Scientific, Singapore, 1993).
- [32] H. J. C. Berendsen, D. van der Spoel, and R. van Drunen, GROMACS: A message-passing parallel molecular dynamics implementation, *Comput. Phys. Commun.* **91**, 43 (1995).
- [33] E. Lindahl, B. Hess, and D. van der Spoel, GROMACS 3.0: A package for molecular simulation and trajectory analysis, *Molec. Model. Annu.* **7**, 306 (2001).
- [34] D. V. D. Spoel, E. Lindahl, B. Hess, G. Groenhof, A. E. Mark, and H. J. C. Berendsen, GROMACS: Fast, flexible, and free, *J. Comput. Chem.* **26**, 1701 (2005).
- [35] B. Hess, C. Kutzner, D. van der Spoel, and E. Lindahl, GROMACS 4: Algorithms for highly efficient, load-b, and scalable molecular simulation, *J. Chem. Theory Comput.* **4**, 435 (2008).
- [36] M. Parrinello and A. Rahman, Polymorphic transitions in single crystals: A new molecular dynamics method, *J. Appl. Phys.* **52**, 7182 (1981).
- [37] S. Nosé and M. L. Klein, Constant pressure molecular dynamics for molecular systems, *Mol. Phys.* **50**, 1055 (1983).
- [38] G. Bussi, D. Donadio, and M. Parrinello, Canonical sampling through velocity rescaling, *J. Chem. Phys.* **126**, 014101 (2007).
- [39] B. J. Palmer, Transverse-current autocorrelation-function calculations of the shear viscosity for molecular liquids, *Phys. Rev. E* **49**, 359 (1994).
- [40] B. Hess, Determining the shear viscosity of model liquids from molecular dynamics simulations, *J. Chem. Phys.* **116**, 209 (2002).
- [41] G.-J. Guo and Y.-G. Zhang, Equilibrium molecular dynamics calculation of the bulk viscosity of liquid water, *Mol. Phys.* **99**, 283 (2001).
- [42] Y. Wu, H. L. Tepper, and G. A. Voth, Flexible simple point-charge water model with improved liquid-state properties, *J. Chem. Phys.* **124**, 024503 (2006).
- [43] T. Chen, B. Smit, and A. T. Bell, Are pressure fluctuation-based equilibrium methods really worse than nonequilibrium methods for calculating viscosities? *J. Chem. Phys.* **131**, 246101 (2009).
- [44] G. Guevara-Carrion, J. Vrabec, and H. Hasse, Prediction of self-diffusion coefficient and shear viscosity of water and its binary mixtures with methanol and ethanol by molecular simulation, *J. Chem. Phys.* **134**, 074508 (2011).
- [45] C. Eckart, Some studies concerning rotating axes and polyatomic molecules, *Phys. Rev.* **47**, 552 (1935).
- [46] M. A. González and J. L. F. Abascal, The shear viscosity of rigid water models, *J. Chem. Phys.* **132**, 096101 (2010).
- [47] J. R. Tyldesley, *An Introduction to Tensor Analysis for Engineers and Applied Scientists* (Longman, London, 1975).
- [48] T. M. Squires and T. G. Mason, Tensorial generalized Stokes-Einstein relation for anisotropic probe microrheology, *Rheol. Acta* **49**, 1165 (2010).
- [49] Y. von Hansen, Stochastic dynamics in biomolecular systems, Ph.D. thesis, Freie Universität Berlin, 2014.
- [50] I.-C. Yeh and G. Hummer, System-s dependence of diffusion coefficients and viscosities from molecular dynamics simulations with periodic boundary conditions, *J. Phys. Chem. B* **108**, 15873 (2004).
- [51] M. Linke, J. Köfinger, and G. Hummer, Rotational diffusion depends on box size in molecular dynamics simulations, *J. Phys. Chem. Lett.* **9**, 2874 (2018).
- [52] L. Scalfi, D. Vitali, H. Kiefer, and R. R. Netz, Frequency-dependent hydrodynamic finite size correction in molecular simulations reveals the long-time hydrodynamic tail, *J. Chem. Phys.* **158**, 191101 (2023).
- [53] J. C. F. Schulz, A. Schlaich, M. Heyden, R. R. Netz, and J. Kappler, Molecular interpretation of the non-Newtonian viscoelastic behavior of liquid water at high frequencies, *Phys. Rev. Fluids* **5**, 103301 (2020).
- [54] J. Qvist, C. Mattea, E. P. Sunde, and B. Halle, Rotational dynamics in supercooled water from nuclear spin relaxation and molecular simulations, *J. Chem. Phys.* **136**, 204505 (2012).
- [55] A. Dehaoui, B. Issenmann, and F. Caupin, Viscosity of deeply supercooled water and its coupling to molecular diffusion, *Proc. Natl. Acad. Sci. USA* **112**, 12020 (2015).
- [56] I. N. Tsimpanogiannis, S. H. Jamali, I. G. Economou, T. J. H. Vlught, and O. A. Moulton, On the validity of the Stokes-Einstein relation for various water force fields, *Mol. Phys.* **118**, e1702729 (2020).
- [57] M. G. Mazza, N. Giovambattista, H. E. Stanley, and F. W. Starr, Connection of translational and rotational dynamical heterogeneities with the breakdown of the Stokes-Einstein and Stokes-Einstein-Debye relations in water, *Phys. Rev. E* **76**, 031203 (2007).
- [58] H. Kiefer, D. Vitali, B. A. Dalton, L. Scalfi, and R. R. Netz, Effect of frequency-dependent viscosity on molecular friction in liquids, [arXiv:2408.12506](https://arxiv.org/abs/2408.12506).
- [59] N. Kavokine, R. R. Netz, and L. Bocquet, Fluids at the nanoscale: From continuum to subcontinuum transport, *Annu. Rev. Fluid Mech.* **53**, 377 (2021).
- [60] B. C. Carlson, Numerical computation of real or complex elliptic integrals, *Numer. Algor.* **10**, 13 (1995).
- [61] B. C. Carlson and J. FitzSimons, Reduction theorems for elliptic integrands with the square root of two quadratic factors, *J. Comput. Appl. Math.* **118**, 71 (2000).
- [62] D. van der Spoel and P. J. van Maaren, The origin of layer structure artifacts in simulations of liquid water, *J. Chem. Theory Comput.* **2**, 1 (2006).
- [63] T. Al-Shemmeri, *Engineering Fluid Mechanics* (Ventus, Erie, CO, 2012).